JACS
JOURNAL OF THE AMERICAN CHEMICAL SOCIETY

Article

pubs.acs.org/JACS

Meta-Atom Behavior in Clusters Revealing Large Spin Ground States

Raúl Hernández Sánchez and Theodore A. Betley*

Department of Chemistry and Chemical Biology, Harvard University, 12 Oxford Street, Cambridge, Massachusetts 02138, United States

Supporting Information

ABSTRACT: The field of single molecule magnetism remains predicated on super- and double exchange mechanisms to engender large spin ground states. An alternative approach to achieving high-spin architectures involves synthesizing weak-field clusters featuring close M−M interactions to produce a single valence orbital manifold. Population of this orbital manifold in accordance with Hund's rules could potentially yield thermally persistent high-spin ground states under which the valence electrons remain coupled. We now demonstrate this effect with a reduced hexanuclear iron cluster that achieves an $S = 19/2$ ($\chi_M T \approx 53$ cm^3 K/mol) ground state that persists to 300 K, representing the largest spin ground state persistent to room temperature reported to date. The reduced cluster displays single molecule magnet behavior manifest in both variable-temperature zero-field ^{57}Fe Mössbauer and magnetometry with a spin reversal barrier of 42.5(8) cm^{-1} and a magnetic blocking temperature of 2.9 K (0.059 K/min).

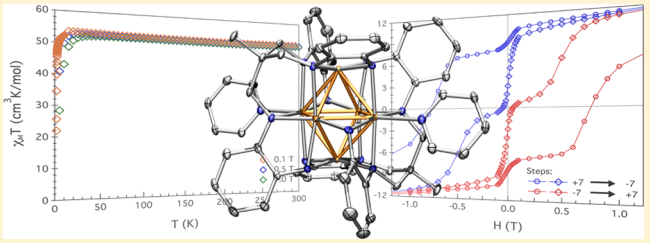

1. INTRODUCTION

To achieve technological viability (operational temperatures approaching 298 K) using single molecule magnets (SMM), new synthetic strategies must be deployed to overcome the thermal limitations with the existing state of the art SMM materials.[1] Two basic requirements for manifesting single molecule magnet behavior with a large spin reversal barrier (U) are (1) a high-spin ground state (S) and (2) large magnetic anisotropy.[2] To address the former, researchers have approached maximizing the molecular spin ground state by synthesizing large polynuclear assemblies wherein clusters of paramagnetic ions couple their spins via superexchange pathways to achieve extraordinary spin ground states ($S = 7 \rightarrow 83/2$).[3−23] However, as a result of the superexchange coupling mechanism employed, the maximum high-spin regime for the cited examples only manifests at low temperatures ($T <$ ~30 K), above which the superexchange interaction is thermally overcome and the metal centers behave as magnetically noninteracting. Stronger electronic alignment of the paramagnetic centers can be engendered by employing radicaloid ligands that facilitate ferrimagnetic spin alignment[24] and by spin delocalization in mixed valent clusters where the double exchange mechanism is operative, wherein two metals of different oxidation state come into strong electronic alignment to facilitate internuclear electron exchange.[25] Indeed, clusters employing these exchange mechanisms have been shown to exhibit thermally well-isolated ground states that persist even to room temperature and beyond,[26] though systematic manipulation of the magnetic anisotropy remains elusive. To improve SMM properties to achieve technical viability, new materials exhibiting facile electronic exchange are necessary to maximize spin ground states while also providing a systematic means for manipulating magnetic anisotropy.[27]

An alternative approach to achieving strong electronic coupling between paramagnetic centers is through the generation of clusters featuring direct M−M bonding interactions to facilitate direct intracluster valence orbital overlap. In the strong field limit where the M−M overlap is sterically unimpeded, maximal pairing of the valence electrons can occur to yield maximal M−M bond orders (BO = 1−5) and covalency is maximized.[28] In the weak field limit where energetic separation between valence orbitals is less than the mean electron pairing energy for a transition element, the valence electrons will populate in a parallel alignment to achieve a high-spin configuration in accordance with Hund's rules. Targeting weak field clusters requires management of both metal−ligand (use of weak field ancillary ligands) and metal−metal interactions (sterically preclude strong M−M bond formation). If these conditions are met, the transition-metal valence orbitals will mix according to symmetry, creating a single d-orbital manifold approximating that of a single metal ion.[29] Indeed, maximally high-spin complexes for iron have been achieved for dinuclear $S = 4$ $(DPhF)_4Fe_2$,[30] $S = 9/2$ $[(Me_3tacn)_2Fe_2(\mu^2\text{-}OH)_3]^{2+}$,[26a,b,e] $S = 9/2$ $[Fe_2(\mu\text{-}O_2CAr^{Tol})_4(py)_2]^+$,[31] and $S = 6$ trinuclear $(^{tbs}L)Fe_3(thf)$[32] and $(^{Ph}L)Fe_3(thf)_3$[33] dictated by this direct exchange pathway. We now demonstrate that chemical reduction of the intermediate spin hexanuclear cluster $(^{H}L)_2Fe_6$ (**1**)[34] induces an abrupt increase in its electronic configuration to achieve a thermally persistent $S = 19/2$ spin ground state which displays SMM behavior at low temperature.

Received: August 28, 2015
Published: October 6, 2015

DOI: 10.1021/jacs.5b08962
J. Am. Chem. Soc. 2015, 137, 13949−13956

2. EXPERIMENTAL SECTION

2.1. General Considerations. All manipulations involving metal complexes were carried out using standard Schlenk or glovebox techniques under a dinitrogen atmosphere, unless otherwise noted. All glassware was oven-dried for a minimum of 10 h and cooled in an evacuated chamber prior to use in the drybox. Diethyl ether and tetrahydrofuran (THF) were dried and deoxygenated on a Glass Contour System (SG Water USA, Nashua, NH) and stored over 4 Å molecular sieves (Strem) prior to use. Pyridine (Sure/Seal) and *N*,*N*-dimethylformamide (Sure/Seal) were purchased from Sigma-Aldrich and stored over 4 Å sieves prior to use. Nonhalogenated solvents were frequently tested, by a solution of sodium benzophenone ketyl in THF, for effective water and dioxygen removal. Tetrabutylammonium chloride was purchased from Sigma-Aldrich and naphthalene from Alfa Aesar and used without further purification. $(^{H}L)_2Fe_6$ (**1**) was prepared according to the methodology previously reported by our laboratory.[34]

*2.1.1. $[Bu_4N][(^{H}L)_2Fe_6(py)_2]$ (**2**).* $(^{H}L)_2Fe_6$ (**1**) (100 mg, 0.080 mmol) was suspended in 2 mL of THF and cooled down to −35 °C. A freshly prepared solution of sodium naphthalenide (10.3 mg of naphthalene, 0.080 mmol) in 2 mL of THF (−35 °C) was added to the suspension of $(^{H}L)_2Fe_6$ (**1**) by filtering through Celite. Immediately following combination of the solutions, $[Bu_4N]Cl$ (22.4 mg, 0.080 mmol) was added as a solid, and the reaction mixture was stirred for 3 h at room temperature. The dark brown precipitate was collected upon a medium size fritted funnel and washed with 5 × 2 mL of THF. The solid left behind was extracted into pyridine, and the dark brown solution extracted through the fritted funnel into a diethyl ether vapor diffusion cell. Bulk crystallization provides **2** in 48% yield (average over several batches). Anal. calcd for **2**: $C_{72}H_{94}Fe_6N_{15}$: C, 57.47; H, 6.30; N, 13.96%. Found: C, 57.28; H, 6.41; N, 13.86%.

*2.1.2. $[Bu_4N][(^{H}L)_2Fe_6(dmf)_2]$ (**3**).* The preparation of **3** is identical to that of **2** the only difference is that instead of extracting with pyridine, *N*,*N*-dimethylformamide (dmf) is used. Similarly, the dark brown solution is extracted through the fritted funnel into a diethyl ether vapor diffusion cell. Bulk crystallization provides **3** in 36% yield. Anal. calcd for **3**: $C_{68}H_{98}Fe_6N_{15}O_2$: C, 54.72; H, 6.62; N, 14.08%. Found: C, 54.58; H, 6.65; N, 13.91%.

2.2. X-ray Structure Determinations. Single crystals suitable for X-ray structure analysis were coated with deoxygenated Paratone N-oil and mounted in MiTeGen Kapton loops (polyimide). Data for compound **2** were collected using synchrotron radiation at the Argonne National Laboratory Advance Photon Source, ChemMatCARS. Data for compound **3** were collected at 100 K on an APEX II DUO single crystal diffractometer. None of the crystals showed significant decay during data collection. Raw data were integrated and corrected for Lorentz and polarization effects using Bruker APEX2 v.2009.1.[35] Absorption corrections were applied using SADABS.[36] Space group assignments were determined by examination of systematic absences, E-statistics, and successive refinement of the structures. The program PLATON[37] was employed to confirm the absence of higher symmetry for any of the crystals. The positions of the heavy atoms were determined using direct methods using the program SHELXTL.[38] Successive cycles of least-squares refinement followed by difference Fourier syntheses revealed the positions of the remaining non-hydrogen atoms. Non-hydrogen atoms were refined with anisotropic displacement parameters, and hydrogen atoms were added in idealized positions. Crystallographic data for **2** and **3** are given in Table S1.

2.3. Magnetic Data Measurements. Magnetic data for **1**, **2**, and **3** were collected using a Quantum Design MPMS-XL Evercool SQUID magnetometer. The following is a general procedure for sample preparation: bulk crystals were collected and washed thoroughly with Et_2O. These black block-shaped crystals were crushed in the presence of Et_2O, and the resulting fine suspension was then dried under high vacuum. The sample powder was then immobilized within a gelatin capsule size no. 4 by adding melted eicosane at 50−60 °C. The gelatin capsule was inserted into a plastic straw. Samples were prepared under a dinitrogen atmosphere. Magnetization data at 100 K from 0 to 7 T were used as a test for ferromagnetic impurities (see Figures S11−13). Variable-temperature (VT) direct current (dc) magnetic susceptibility measurements were collected in the temperature range 1.8−300 K under applied fields of 0.1, 0.5, and 1 T. The $\chi_M T$ data were collected multiple times until they were reproduced at least three times (in all three cases the ferromagnetic-impurity test was passed). Variable-temperature, variable-field (VTVH) magnetization data were acquired on heating from 1.8 to 10 K at increasing fields of 1, 2, 3, 4, 5, 6, and 7 T. Magnetic susceptibility data were corrected for diamagnetism of the sample, estimated using Pascal's constants,[39] in addition to contributions from the sample holder and eicosane. The ac magnetic susceptibility data were collected at zero applied dc field and with a 4 Oe oscillating ac field. Magnetization data were collected at 1.8 K on steps and cycling between −7 and +7 T to probe for magnetic hysteresis. Additionally, zero-field-cooled (ZFC) and field-cooled (FC) data were collected between 1.8 and 10 K by measuring with a dc applied field of 0.1 T and at a sweeping rate of 0.059 K/min.

2.4. Fitting the Magnetic Data for 1−3. The VT magnetic susceptibility and the VTVH magnetization data were fit in *PHI*[40] according to the spin Hamiltonians described in the main text. The relaxation dynamics were fit according to a generalized Debye model.[41] Igor Pro Wavemetrics was used to fit χ_M'' and χ_M' vs ν to a distribution of single relaxation processes; similarly, it was also used to fit χ_M'' vs T as described elsewhere.[42]

2.5. Electrochemical Measurements. Cyclic voltammetry measurements were acquired by a CHI660d potentiostat using a three-electrode cell with a glassy carbon working electrode, platinum wire as a counter electrode, and a $Ag/AgNO_3$ reference electrode. All potentials were referenced versus the Fc/Fc^+ couple. Saturated $AgNO_3$ solutions were prepared fresh before each experiment. A 0.1 M solution of tetrabutylammonium hexafluorophosphate in pyridine was employed as a supporting electrolyte. All measurements were done under a dinitrogen atmosphere.

2.6. Zero-Field ^{57}Fe Mössbauer Spectroscopy. Data were previously reported for **1** at 90 K only;[34] thus the 4.2 K spectrum was recorded (Figure S3). Data for **2** and **3** were acquired at 4.2, 90, and 210 K. Solid samples (ca. 20 mg) were restrained with Paratone-N oil. The data were measured with a constant acceleration spectrometer (SEE Co., Minneapolis, MN). Isomer shifts are given relative to α-Fe metal at 298 K.

2.7. Other Physical Measurements. Elemental analysis was performed by Complete Analysis Laboratories, Inc., Parsippany, New Jersey. Perpendicular mode X-band EPR spectra were collected in 2-methyltetrahydrofuran at several different temperatures from 3.2 to 79 K on a Bruker ElexSys E500 EPR spectrometer. UV−vis-NIR spectra were collected in a 1 cm path length cuvettes on a Varian 5000 UV−vis-NIR spectrophotometer at room temperature. All solutions were prepared in the glovebox, and the cuvettes sealed with a J-Young screw cap. Absorbance values were kept under 1 for all concentrations measured.

3. RESULTS AND DISCUSSION

3.1. Synthesis and Characterization. Reduction of $(^{H}L)_2Fe_6$[34] (**1**) involves adding freshly prepared sodium naphthalenide to a suspension of **1** in THF at −35 °C (Scheme 1). Immediately after combining the two solutions, 1 equiv of $[Bu_4N]Cl$ was added and stirred for 3 h at room temperature during which time a dark brown precipitate forms. Cation metathesis eliminates complications arising from cation desolvation from the previous preparation. The isolated powder was dissolved in pyridine (py) or dimethylformamide (dmf) and set up to crystallize in a vapor diffusion cell containing diethyl ether. Large block-shaped crystals can be obtained at room temperature that affords crystalline $[Bu_4N][(^{H}L)_2Fe_6(py)_2]$ (**2**, 48%) or $[Bu_4N][(^{H}L)_2Fe_6(dmf)_2]$ (**3**, 36%) as room temperature stable materials under an inert atmosphere (Figure 1a). The constitution of **2** and **3** were confirmed by X-ray crystallography (*vide infra*). The solid- and

DOI: 10.1021/jacs.5b08962
J. Am. Chem. Soc. 2015, 137, 13949−13956

Scheme 1

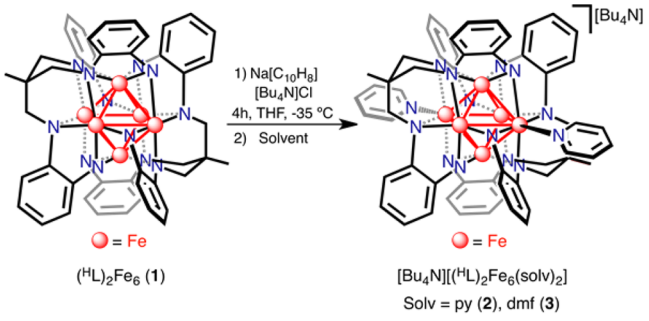

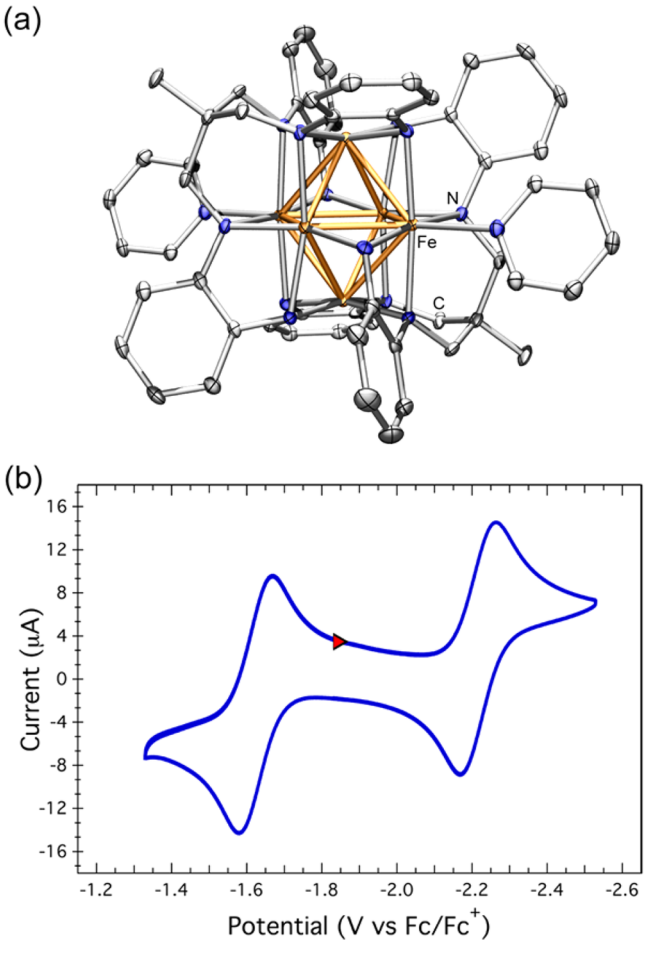

Figure 1. Representative molecular crystal structure and electrochemical behavior of $[Bu_4N][(^HL)_2Fe_6(solv)_2]$. (a) X-ray structure of the cluster anion in **2**. Thermal ellipsoids are set at 50% probability level. The Fe, C, and N atoms are colored orange, gray, and blue, respectively. (b) Cyclic voltammogram of **2** in pyridine at room temperature. Scan rate: 100 mV/s. A 0.1 M $[Bu_4N][PF_6]$ solution was used as supporting electrolyte.

solution-state properties for **2** and **3** are largely analogous, thus properties for the pyridine complex **2** will be discussed in the text, while the comparable data for **3** are presented in the Supporting Information.

Unlike the unsolvated cluster **1**, the X-ray molecular crystal structures of the anionic clusters **2** and **3** display *trans*-ligation of solvent to make the $[Fe_6]$ octahedron asymmetric as illustrated in Figure 1a. The molecular crystal structure of **2** reveals that the pyridine-bound (d_{Fe-py}: 2.363(3) Å), five-coordinate Fe sites in **2** extend away from the center of the $[Fe_6]$ core (d_{Fe-Fe}: 4.001(2) Å), while the remaining pairs of *trans*-disposed iron sites reveal further asymmetry (d_{Fe-Fe}: 3.403(2), 3.838(2) Å). The *trans*-disposed iron sites in **3** reveal a less significant distortion (d_{Fe-Fe}: 3.442(1), 3.846(1), 3.863(1) Å). Elongation of the Fe−N ligand bonds from **1** (Fe−N 2.037(8), Fe−NH 1.998(2) Å)[34] occurs upon reduction (Fe−N 2.12(3), Fe−NH 2.07(3) Å in **2** and **3**) (see Table 1).

Table 1. Relevant Bond Lengths and Angles for $[(^HL)_2Fe_6]^n$ Species

(Å;°)	**1**[a]	Na[**1**][a]	**2**	**3**
Fe−Fe	2.597(1)	2.580(6)	2.65(4)	2.63(3)
Fe−N	2.037(8)	2.081(8)	2.12(3)	2.11(3)
Fe−NH	1.998(17)	2.052(15)	2.07(3)	2.07(3)
∠Fe−N−Fe	79.2(2)	77.0(2)	78(3)	78(3)
∠Fe−NH−Fe	81.1(2)	77.5(3)	79(2)	78(2)

[a]Previously reported neutral **1** and reduced clusters Na[**1**] (where Na[**1**] = $[Na(Et_2O)_2(NCMe)_2][(^HL)_2Fe_6]$).[34]

To assess the stability of the mixed valence cluster **2**, the electrochemical properties of **2** were investigated via cyclic voltammetry. In pyridine **2** displays one reversible oxidation ($E_{1/2}$ = −1.62 V vs Fc/Fc^+, ΔE_P = 91 mV) and one reversible reduction ($E_{1/2}$ = −2.21 V vs Fc/Fc^+, ΔE_P = 90 mV) as shown in Figure 1b. The reversible reduction at −2.21 V suggests a pyridine-bound, dianionic cluster could be chemically accessible. The calculated comproportionation constant for **2** is 1.3 × 10^{10}, indicating significant electron delocalization in the mixed-valent cluster **2**.[34]

3.2. Zero-Field ^{57}Fe Mössbauer Spectroscopy. Our lab has previously reported the species $[Na(Et_2O)_2(NCMe)_2][(^HL)_2Fe_6]$ having an asymmetric ^{57}Fe Mössbauer spectrum at 90 K.[34] The spectral asymmetry was attributed to a proposed mixture of neutral $(^HL)_2Fe_6$ and reduced $[Na(Et_2O)_2(NCMe)_2][(^HL)_2Fe_6]$ clusters, owing to the presumed instability of the $[Fe_6]^-$. An alternative reason for the spectral asymmetry could be due to slow magnetic relaxation of the $[Fe_6]^-$ that is not fully resolved at 90 K.[44] Thus, samples of polycrystalline **2** were isolated, and their Mössbauer spectra recorded at 4.2 K under a zero-applied external magnetic field.

The spectrum of the pyridine adduct **2** features a well-defined multiline pattern at 4.2 K (Figure 2a). The data were modeled taking into account three crystallographically distinct iron environments. The zero-field spectrum was modeled by employing a nuclear Hamiltonian that only includes the electric quadrupole and the nuclear Zeeman interaction: $\hat{H} = \mathbf{I}\cdot Q\cdot\mathbf{I} + g_n\beta_n\mathbf{H}\cdot\mathbf{I}$,[45] where Q is proportional to the electric field gradient. The only contribution to $\mathbf{H}$ originates from the internal magnetic field ($\mathbf{H}_{int}$) since $\mathbf{H}_{ext}$ = 0. In this case, the "static" internal field ($\mathbf{H}_{int}$) results from slow relaxation of the electronic ground state $|S, m_s\rangle$.[46] The data were fit as described in the Supporting Information. The three sextets that best model the data have the following parameters [δ, ΔE_Q (mm/s), $\mathbf{H}_{int}$ (T): 0.55, +0.15, 36.6 (33%, blue trace); 0.65, −0.06, 39.1 (33%, green trace); and 0.80, 0.72, 34.6 (34%, brown trace)] and are shown in Figures 2a and S4. The hyperfine splitting disappears upon warming to 90 K, but relaxation effects are still observed (Figure 2b). In the high-temperature regime the internal field relaxes fast enough to average to zero, and thus the only perturbation that persists is the quadrupole

DOI: 10.1021/jacs.5b08962
J. Am. Chem. Soc. 2015, 137, 13949−13956

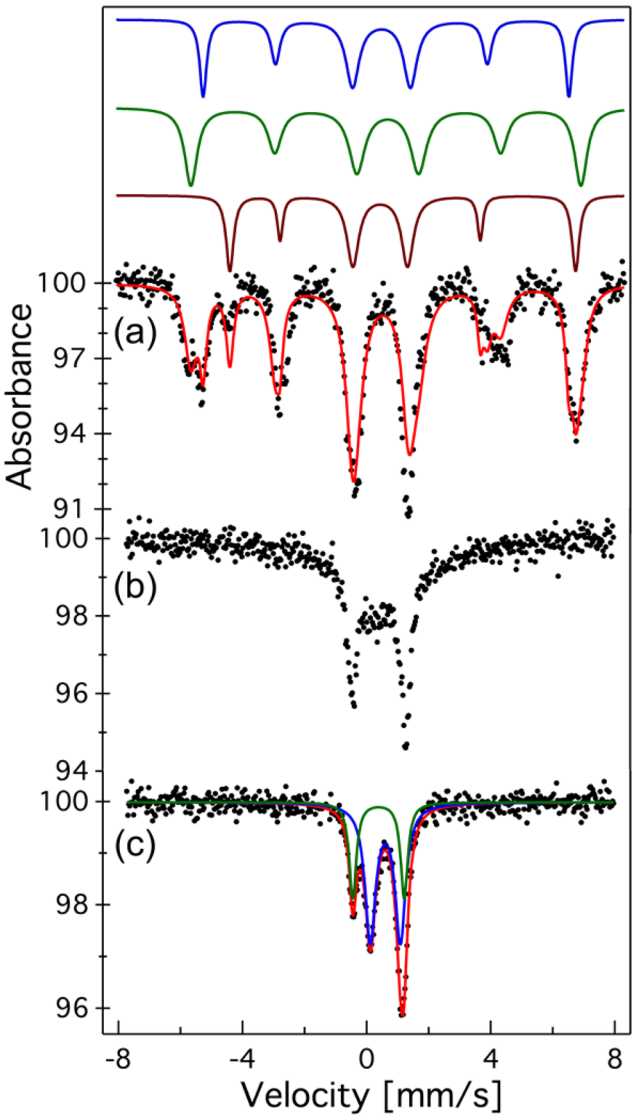

Figure 2. Zero-field ^{57}Fe Mössbauer spectra for $[Bu_4N][(^{H}L)_2Fe_6(py)_2]$. Spectra collected at: (a) 4.2, (b) 90, and (c) 210 K. The red traces in (a) and (c) correspond to the overall fit. The fit in (a) is composed of three sextets shown by the top blue, green, and brown traces; similarly, the fit in (c) encompasses the two doublets shown in blue and green. The fit parameters are described in the text.

interaction.[47] Two sharp doublets are observed at 210 K (Figure 2c) with Mössbauer parameters [δ, $|\Delta E_Q|$ (mm/s): 0.61, 0.97 (59%, blue trace); 0.38, 1.65 (41%, green trace)]. Hence, while the 4.2 K data reflect three distinct iron sites (consistent with the crystallographic data), the four four-coordinate sites become equivalent as temperature increases, distinct only from the pyridine bound five-coordinate iron sites.

3.3. Magnetometry. Variable-temperature (VT) magnetic susceptibility (χ_MT) data and VTVH magnetization data were collected for compounds **2** and **3** to assess their spin ground states. The χ_MT data for **2** obtained at 0.1 T from 1.8 to 300 K are shown in Figure 3a, which indicates a well-isolated ground state up to room temperature. At 50 K χ_MT has a maximum of 55.94 cm^3 K/mol ($\chi_M T_{50\ K}$ = 53.39 cm^3 K/mol for **3**, Figure S15a); which decreases to 52.54 cm^3 K/mol at 300 K.[48] Below 50 K the effect of zero-field splitting is manifest and χ_MT drops rapidly until 3 K (46.50 cm^3 K/mol), after which it falls precipitously to 2.23 cm^3 K/mol at 1.8 K (Figure S14). The susceptibility data for **2** was fit between 5 and 150 K using *PHI*[49] according to the spin Hamiltonian $\hat{H} = D\hat{S}_z^2 + g_{iso}\mu_B \mathbf{S}\cdot\mathbf{H}$ for an S = 19/2 ground state to give: g = 2.11 and $|D|$ = 0.67 cm^{-1}. Similarly for **3**: g = 2.06 and $|D|$ = 0.40 cm^{-1} for an S = 19/2.[50] These parameters were utilized to extrapolate the fit to 300 K. The susceptibility data for **1** are also shown for means of comparison to the intermediate spin S = 6 configuration. The VTVH magnetization data for **2** nearly plateau as the magnetic field is increased, indicating full population of the spin ground state saturating at 16.5 μ_B (17.0 μ_B for **3**, Figure S18) at 1.8 K and 7 T (Figure 3b). An ideal S = 19/2 (g = 2.0) would be expected to saturate at 19 μ_B, while deviation from saturation at the $M = gS$ limit can be attributed to the presence of zero-field splitting. The reduced magnetization data of **2** were fit according to the spin Hamiltonian $\hat{H} = D\hat{S}_z^2 + E(\hat{S}_x^2 - \hat{S}_y^2) + g_{iso}\mu_B \mathbf{S}\cdot\mathbf{H}$ to yield the following parameters for the S = 19/2 ground state: g = 2.10, D = −0.60, and $|E/D|$ = 0.30 (Figure 3b). Fitting of **3** as an S = 19/2 in an analogous way to **2** we obtain g = 2.06, D = −0.48, and $|E/D|$ = 0.24 (Figure S18). Analysis of the χ_M'T vs T dependence for **2**, where population of low-lying excited states under large dc fields is suppressed,[51] reveals a plateau of 53 cm^3 K/mol in χ_M'T for T > 5 K (Figure 3c), in agreement with the expected value for an ideal S = 19/2 (g = 2, χ_MT = 49.875 cm^3 K/mol).

The low-temperature slow magnetic relaxation evident from the Mössbauer spectrum of **2** and the precipitous drop in susceptibility led us to examine whether magnetic blocking was operative. Thus, zero-field-cooled (ZFC) and field-cooled (FC) magnetization data were collected at 0.059 K/min for **2**. The ZFC data at 0.1 T display a narrow peak on the magnetization at 2.9 K; in contrast the FC data display no peak but rather a plateau at 3.07(1) μ_B from 1.8 to 2.5 K, after which the moment decreases superimposing with the ZFC data at $T \geq$ 3.0 K (inset Figure 3c), a signature of magnetic blocking.[3a]

3.4. Slow Magnetic Relaxation. The relaxation dynamics of **2** were further probed by ac magnetic susceptibility at a 4 Oe oscillating field (1−1488 Hz) and in the absence of an external dc magnetic field in the temperature range 1.8−6.6 K. A maximum in the out-of-phase component (χ_M'' vs ν, Figure 4a) and the concurrent decrease in the in-phase component (χ_M' vs ν, Figure 4c) are hallmark characteristics of slow magnetic relaxation. The maximum in χ_M'' vs ν occurs in a narrow temperature range (3.4 to 6.6 K) and is consistent with the sharp maximum observed in the ZFC data.[24a] Alternatively, the relaxation behavior can also be observed by a peak maximum in the χ_M'' vs T plot (Figure 4b). Additionally, Cole−Cole plots (χ_M'' vs χ_M') displaying semicircular profiles, as is the case for **2** as illustrated in Figure 4d, indicate that a single relaxation pathway is operative. The relaxation dynamics were fit as described in the Supporting Information to a generalized Debye model.[41] Each panel in Figure 4a−d was fit independently, and the extracted temperature-dependent relaxation times (τ) fit to an Arrhenius temperature law, $\tau = \tau_0 \exp(U_{eff}/k_B T)$. The average values from all the four methods fit to an effective spin relaxation barrier of U_{eff} = 42.5(8) cm^{-1} and an attempt time of $\tau_0 = 9(2) \times 10^{-9}$ s (Figure 4e). Remarkably, parallel analysis of the less structurally distorted dmf-ligated cluster **3** reveals a lower effective spin relaxation barrier of U_{eff} = 33.5(1) cm^{-1} and an attempt time of $\tau_0 = 1.3(1) \times 10^{-8}$ s (Figure 4e). The magnetic blocking temperature (T_B) is 2.9 K from examination of the ZFC data (Figure 3c inset). Magnetic hysteresis experiments were conducted on **2** at 1.8 K (Figure 4f) where step-like behavior is observed as the magnetization at ±7 T

DOI: 10.1021/jacs.5b08962
J. Am. Chem. Soc. 2015, 137, 13949−13956

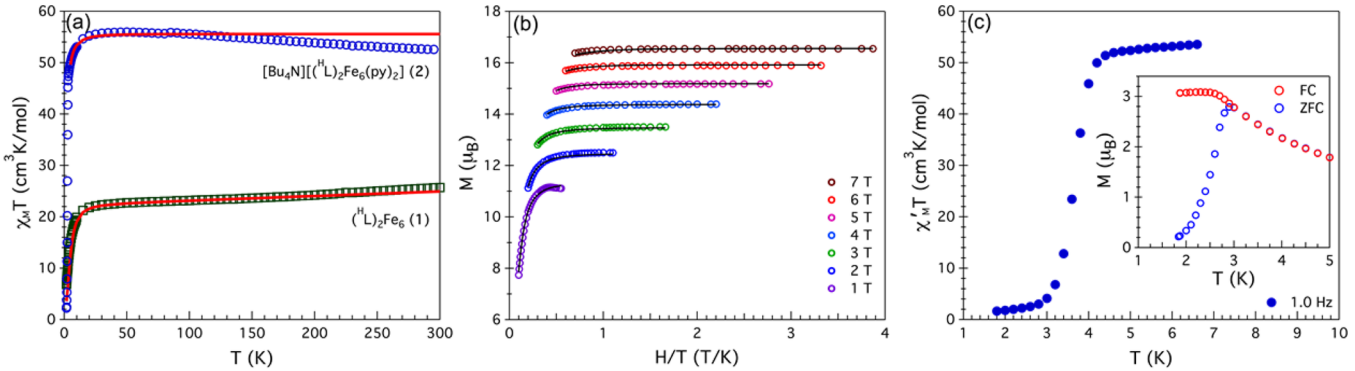

Figure 3. Magnetic characterization of $(^{H}L)_2Fe_6$ and $[Bu_4N][(^{H}L)_2Fe_6(py)_2]$. (a) VT dc magnetic susceptibility of **1** (1 T, green squares) and **2** (0.1 T, blue circles). (b) VTVH magnetization of **2** at selected fields (1−7 T) measured on increasing temperature from 1.8 to 10 K. Solid red and black lines in (a) and (b) correspond to the fit of the data as described in the text, respectively. (c) Plot of $\chi_M'T$ versus T for **2** at an oscillating field frequency of 1 Hz. The inset displays the ZFC and FC data of **2** collected between 1.8 and 5 K at 0.1 T and at a temperature sweeping rate of 0.059 K/min.

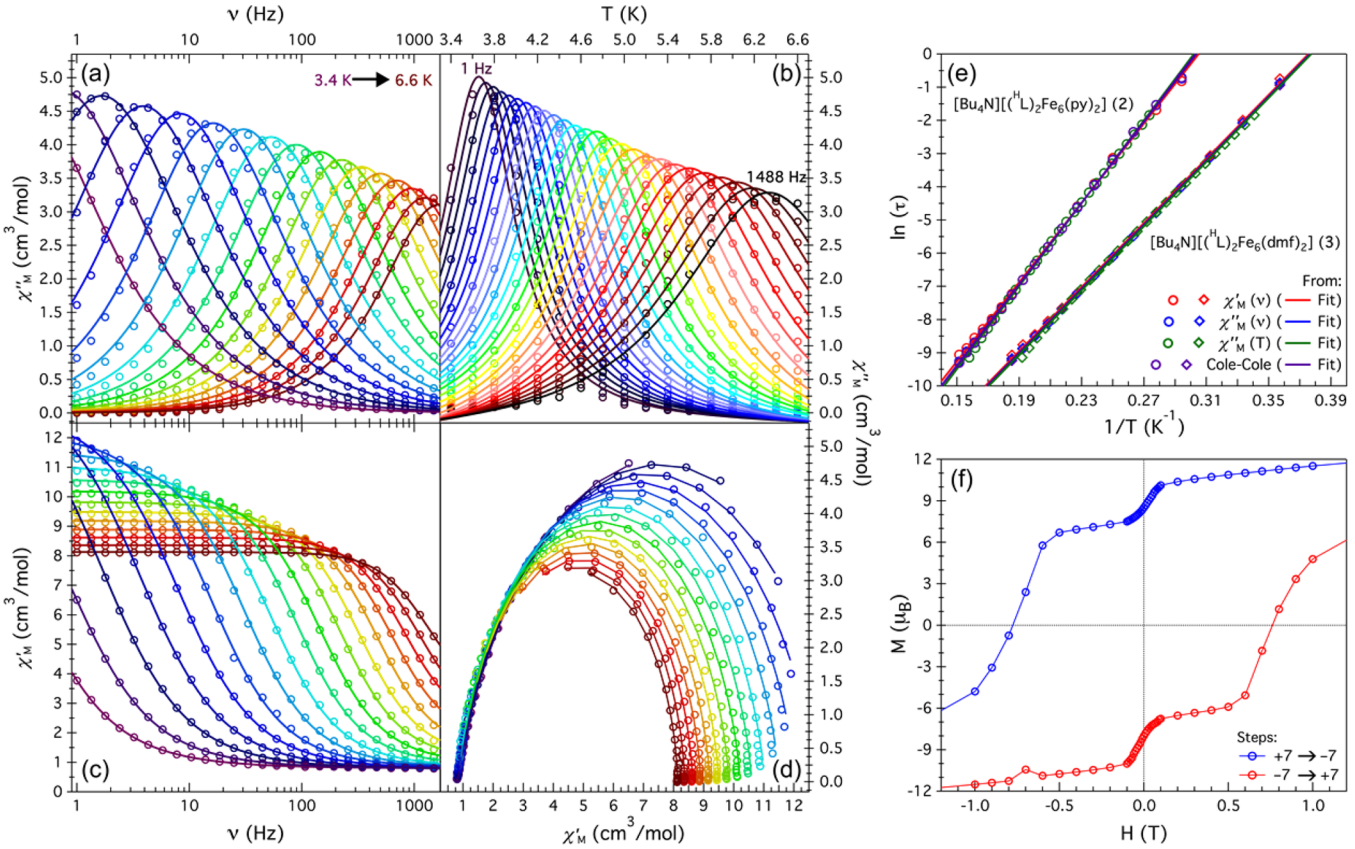

Figure 4. Slow magnetic relaxation phenomena in $[Bu_4N][(^{H}L)_2Fe_6(py)_2]$. Out-of-phase ($\chi_M''$, a) and in-phase ($\chi_M'$, c) components of the ac magnetic susceptibility versus frequency (ν). (b) χ_M'' versus T. (d) Cole−Cole plots. The solid continuous lines in (a−d) represent a fit to the data as described in the text. Data collected under a zero-applied dc field. (e) Relaxation times (ln τ) extracted from (a−d) versus 1/T for **2** (circles) and Figure S21 for **3** (diamonds). (f) Zoomed-in plot of the magnetic hysteresis loop from −7 to +7 T. Data collected at rate, range: 0.296 mT/s, ± 1 ⇆ ± 0.1 T; and 0.041 mT/s, +0.1 ⇆ −0.1 T.

reaches ±16.6 μ_B (Figure S22). A remnant magnetization of 8.5 μ_B is observed when cycling from +7 to −7 T with a coercive field of ∼0.8 T. Step-like hysteresis has been attributed to quantum tunneling of magnetization, one of only a few macroscopic measurements where quantum effects are evident.[52] The current data suggest that ligation of the pyridine molecules in **2** provides a route to impart magnetic anisotropy via the large axial structural distortion. The effective spin reversal barrier in **2** is U_{eff} = 42.5(8) cm^{-1} which is less than the theoretical value calculated from $U = |D|(S^2 - 1/4)$, where S = 19/2 and D = −0.60 cm^{-1} yielding U of 54 cm^{-1}. Similarly for **3** U_{eff} = 33.5(1) cm^{-1} vs the calculated barrier U of 43.2 cm^{-1}. Inclusion of the rhombic ZFS parameter in the calculation of the spin reversal barrier provides U of 60.8 and 46.8 cm^{-1} for **2** and **3**, respectively (see the Supporting Information). The lower than theoretical U_{eff} observed is typical of systems where the spin reversal does not follow strictly the thermal barrier, but

DOI: 10.1021/jacs.5b08962
J. Am. Chem. Soc. 2015, 137, 13949−13956

instead tunnels through the barrier at some higher energy m_s levels.[2,53]

3.5. Electronic Structure Determination. Significant spectroscopic, magnetic, and structural perturbations arise upon reduction of **1** by one electron (*vide supra*). Most remarkably, the spin ground-state changes abruptly from $S = 6$ for the parent all-ferrous cluster **1**, to an $S = 19/2$ for **2** and **3**, for which we sought to account using a delocalized cluster bonding approach.

Previously we proposed a qualitative molecular orbital diagram for **1** to account for the $S = 6$ ground state (Figure 5a).[34] The axis system at each iron site was chosen so that the

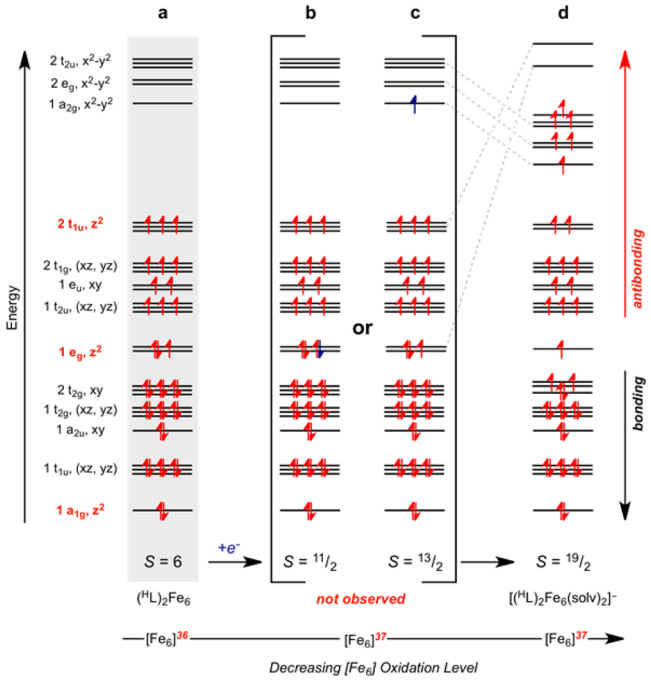

Figure 5. Qualitative molecular orbital diagram derived for hexanuclear iron clusters. Molecular orbital diagram proposed to explain the spin ground state in (a) neutral $(^{H}L)_2Fe_6$[34] and (d) reduced $[(^{H}L)_2Fe_6(solv)_2]^-$ clusters **2** and **3**.

d_{z^2} orbital is oriented normal to the cluster face and the $d_{x^2-y^2}$ orbital along the Fe−N(H) bonds. The frontier iron 3d orbitals were combined based on symmetry considerations and filled with the available 36 iron valence electrons. To account for the observed $S = 6$, the symmetry-adapted linear combinations (SALCs) of the Fe−N antibonding interactions ($1a_{2g}$, $2e_g$, and $2t_{2u}$) are high enough in energy to remain unpopulated (Figure 5a).

Based on the proposed model for $(^{H}L)_2Fe_6$, reduction of **1** could result in two potential scenarios: (1) the added electron fills the $1e_g$ orbital set ($1e_g^4$) to yield an $S = 11/2$ configuration (Figure 5b); or (2) the added electron populates the lowest unoccupied molecular orbital ($1a_{2g}^1$) to yield an $S = 13/2$ configuration (Figure 5c). Although neither scenario is observed, the latter may suggest a pathway through which the actual high-spin ground state is attained. Addition of an electron to any of the $1a_{2g}$, $2e_g$, or $2t_{2u}$ antibonding orbitals would weaken the Fe−N(H) bonds and lower their energy as a result. This is indeed the case and is structurally manifested in the longer Fe−N and Fe−NH bond distances observed for **2** and **3** (Table 1). Furthermore, the lower-lying $1a_{2g}$, $2e_g$, and $2t_{2u}$ orbitals are now energetically accessible to be populated and maximize the electron exchange interaction for the cluster. Thus, we might anticipate that the true ground state of the coordinatively unsaturated species would be a maximally high-spin configuration of $S = 23/2$. While this is yet to be verified, we can account for the observed spin state of the pyridine bound **2** by considering how pyridine ligation alters the frontier orbital picture in Figure 5. Akin to the redox directed binding of acetonitrile or dimethylformamide to $[(^{H}L)_2Fe_6]^+$,[34,54] two nominally d_{z^2}-based SALCs (originating from $1e_g$ and $2t_{1u}$) are destabilized upon binding of solvent to the $[(^{H}L)_2Fe_6]^-$ core, leaving two orbitals out of energetic range to be populated. Thus, populating the 37 valence electrons in the remaining 28 orbitals affords a maximum spin ground state of $S = 19/2$ (Figure 5d) consistent with that determined experimentally, and suggesting ΔE ($2t_{2u}$−$2t_{2g}$) $\leq$ 19150 cm^{-1} (2.37 eV) the mean spin-pairing energy for a ferrous ion.[55] Via the strong electron delocalization apparent in these weak field clusters, the electronic structure begins to approximate that of a single transition-metal ion, facilitating the isolation of the observed ground states from lowest-lying electronic excited states.[54] Consistent with this description, the formally mixed valent **2** does not exhibit intervalence charge-transfer bands in the near-infrared ($12000 > \nu > 5000$ cm^{-1}, Figure S23).

4. CONCLUSIONS

The frontier of single molecule magnet design requires strategies to maximize molecular spin while providing a mechanism to generate large magnetic anisotropy. The weak-field cluster approach described herein suggests a mechanism wherein both criteria can be met. The delocalized electronic structure observed for **2** provides a means for generation of well isolated high-spin ground states with the added advantage that postsynthetic cluster solvation can generate the magnetic anisotropy necessary to enable SMM behavior. While the overall magnetic blocking temperatures and spin reversal barriers of **2** and **3** do not exceed other reported SMMs, the findings presented herein highlight how the symmetry reduction imposed on **2** can tune the magnetic properties of these clusters with the possibility of incorporating the $[Fe_6]^-$ unit into larger assemblies. Further exploration of this design element is currently underway.

■ ASSOCIATED CONTENT

Supporting Information

The Supporting Information is available free of charge on the ACS Publications website at DOI: 10.1021/jacs.5b08962.

X-ray crystal structures, spectra and magnetometry data for complexes **1**−**3** (crystallographic data CCDC 1412714 and 1412715 can also be obtained free at www.ccdc.cam.ac.uk/data_request/cif) (PDF)
Crystallographic data (CIF)

■ AUTHOR INFORMATION

Corresponding Author

*betley@chemistry.harvard.edu

Notes

The authors declare no competing financial interest.

■ ACKNOWLEDGMENTS

This work was supported by a grant from the NIH (GM 098395), DOE (DE-SC0008313), and Harvard University.

DOI: 10.1021/jacs.5b08962
J. Am. Chem. Soc. 2015, 137, 13949−13956

R.H.S. gratefully acknowledges Consejo Nacional de Ciencia y Tecnología (CONACYT) and Fundación México for a doctoral fellowship. T.A.B. is grateful for a George W. Merck Fellowship. R.H.S. Acknowledges Dr. Yu-Sheng Chen for the training provided at the Argonne National Laboratory Advance Photon Source, ChemMatCARS.

REFERENCES

(1) Pedersen, K. S.; Bendix, J.; Clerac, R. *Chem. Commun.* **2014**, *50*, 4396.
(2) Christou, G.; Gatteschi, D.; Hendrickson, D. N.; Sessoli, R. *MRS Bull.* **2000**, *25*, 66.
(3) *S* = 7 (a) Sessoli, R.; Gatteschi, D.; Caneschi, A.; Novak, M. A. *Nature* **1993**, *365*, 141.
(4) *S* = 9 Miyasaka, H.; Nakata, K.; Sugiura, K.; Yamashita, M.; Clerac, R. *Angew. Chem., Int. Ed.* **2004**, *43*, 707.
(5) *S* = 19/2 Koizumi, S.; Nihei, M.; Shiga, T.; Nakano, M.; Nojiri, H.; Bircher, R.; Waldmann, O.; Ochsenbein, S. T.; Güdel, H. U.; Fernandez-Alonso, F.; Oshio, H. *Chem. - Eur. J.* **2007**, *13*, 8445.
(6) *S* = 10 (a) Caneschi, A.; Gatteschi, D.; Sessoli, R.; Barra, A. L.; Brunel, L. C.; Guillot, M. *J. Am. Chem. Soc.* **1991**, *113*, 5873. (b) Delfs, C.; Gatteschi, D.; Pardi, L.; Sessoli, R.; Wieghardt, K.; Hanke, D. *Inorg. Chem.* **1993**, *32*, 3099. (c) Barra, A. L.; Debrunner, P.; Gatteschi, D.; Schulz, C. E.; Sessoli, R. *Europhys. Lett.* **1996**, *35*, 133.
(7) *S* = 12 (a) Caneschi, A.; Gatteschi, D.; Laugier, J.; Rey, P.; Sessoli, R.; Zanchini, C. *J. Am. Chem. Soc.* **1988**, *110*, 2795. (b) Sessoli, R.; Tsai, H. L.; Schake, A. R.; Wang, S.; Vincent, J. B.; Folting, K.; Gatteschi, D.; Christou, G.; Hendrickson, D. N. *J. Am. Chem. Soc.* **1993**, *115*, 1804. (c) Sessoli, R.; Gatteschi, D.; Caneschi, A.; Novak, M. A. *Nature* **1993**, *365*, 141. (d) Friedman, J. R.; Sarachik, M. P.; Tejada, J.; Ziolo, R. *Phys. Rev. Lett.* **1996**, *76*, 3830. (e) Aromi, G.; Claude, J.-P.; Knapp, M. J.; Huffman, J. C.; Hendrickson, D. N.; Christou, G. *J. Am. Chem. Soc.* **1998**, *120*, 2977. (f) Milios, C. J.; Vinslava, A.; Wernsdorfer, W.; Moggach, S.; Parsons, S.; Perlepes, S. P.; Christou, G.; Brechin, E. K. *J. Am. Chem. Soc.* **2007**, *129*, 2754.
(8) *S* = 23/2 Moushi, E. E.; Stamatatos, T. C.; Wernsdorfer, W.; Nastopoulos, V.; Christou, G.; Tasiopoulos, A. J. *Angew. Chem., Int. Ed.* **2006**, *45*, 7722.
(9) *S* = 14 (a) Boyd, P. D. W.; Li, Q.; Vincent, J. B.; Folting, K.; Chang, H. R.; Streib, W. E.; Huffman, J. C.; Christou, G.; Hendrickson, D. N. *J. Am. Chem. Soc.* **1988**, *110*, 8537. (b) Goldberg, D. P.; Caneschi, A.; Lippard, S. J. *J. Am. Chem. Soc.* **1993**, *115*, 9299.
(10) *S* = 29/2 Wang, Z. X.; van Tol, J.; Taguchi, T.; Daniels, M. R.; Christou, G.; Dalal, N. S. *J. Am. Chem. Soc.* **2011**, *133*, 17586.
(11) *S* = 16 (a) Stamatatos, T. C.; Foguet-Albiol, D.; Poole, K. M.; Wernsdorfer, W.; Abboud, K. A.; O'Brien, T. A.; Christou, G. *Inorg. Chem.* **2009**, *48*, 9831. (b) Langley, S. K.; Chilton, N. F.; Moubaraki, B.; Murray, K. S. *Dalton Trans.* **2011**, *40*, 12201.
(12) *S* = 33/2 (a) Powell, A. K.; Heath, S. L.; Gatteschi, D.; Pardi, L.; Sessoli, R.; Spina, G.; Del Giallo, F.; Pieralli, F. *J. Am. Chem. Soc.* **1995**, *117*, 2491. (b) Goodwin, J. C.; Sessoli, R.; Gatteschi, D.; Wernsdorfer, W.; Powell, A. K.; Heath, S. L. *J. Chem. Soc., Dalton Trans.* **2000**, 1835.
(13) *S* = 39/2 Zhong, Z. J.; Seino, H.; Mizobe, Y.; Hidai, M.; Fujishima, A.; Ohkoshi, S.; Hashimoto, K. *J. Am. Chem. Soc.* **2000**, *122*, 2952.
(14) *S* = 22 (a) Stamatatos, T. C.; Abboud, K. A.; Wernsdorfer, W.; Christou, G. *Angew. Chem., Int. Ed.* **2006**, *45*, 4134. (b) Manoli, M.; Johnstone, R. D. L.; Parsons, S.; Maurrie, M.; Affronte, M.; Evangelisti, M.; Brechin, E. K. *Angew. Chem., Int. Ed.* **2007**, *46*, 4456. (c) Stamatatos, T. C.; Abboud, K. A.; Wernsdorfer, W.; Christou, G. *Polyhedron* **2007**, *26*, 2042. (d) Stamatatos, T. C.; Poole, K. M.; Abboud, K. A.; Wernsdorfer, W.; O'Brien, T. A.; Christou, G. *Inorg. Chem.* **2008**, *47*, 5006. (e) Wu, G.; Huang, J.; Sun, L.; Bai, J.; Li, G.; Cremades, E.; Ruiz, E.; Clérac, R.; Qiu, S. *Inorg. Chem.* **2011**, *50*, 8580.
(15) *S* = 23 Low, D. M.; Jones, L. F.; Bell, A.; Brechin, E. K.; Mallah, T.; Rivière, E.; Teat, S. J.; McInnes, E. J. L. *Angew. Chem., Int. Ed.* **2003**, *42*, 3781.
(16) *S* = 25 (z) Shaw, R.; Laye, R. H.; Jones, L. F.; Low, D. M.; Talbot-Eeckelaers, C.; Wei, Q.; Milios, C. J.; Teat, S.; Helliwell, M.; Raftery, J.; Evangelisti, M.; Affronte, M.; Collison, D.; Brechin, E. K.; McInnes, E. J. L. *Inorg. Chem.* **2007**, *46*, 4968.
(17) *S* = 51/2 (a) Larionova, J.; Gross, M.; Pilkington, M.; Andres, H.; Stoeckli-Evans, H.; Güdel, H. U.; Decurtins, S. *Angew. Chem., Int. Ed.* **2000**, *39*, 1605. (b) Murugesu, M.; Habrych, M.; Wernsdorfer, W.; Abboud, K. A.; Christou, G. *J. Am. Chem. Soc.* **2004**, *126*, 4766. (c) Murugesu, M.; Takahashi, S.; Wilson, A.; Abboud, K. A.; Wernsdorfer, W.; Hill, S.; Christou, G. *Inorg. Chem.* **2008**, *47*, 9459.
(18) *S* = 26 Charalambous, M.; Moushi, E. E.; Papatrianafyllopoulou, C.; Wernsdorfer, W.; Nastopoulos, V.; Christou, G.; Tasiopoulos, A. J. *Chem. Commun.* **2012**, *48*, 5410.
(19) *S* = 28 Nayak, S.; Beltran, L. M. C.; Lan, Y.; Clérac, R.; Hearns, N. G. R.; Wernsdorfer, W.; Anson, C. E.; Powell, A. K. *Dalton Trans.* **2009**, 1901.
(20) *S* = 61/2 (a) Stamatatos, T. C.; Abboud, K. A.; Wernsdorfer, W.; Christou, G. *Angew. Chem., Int. Ed.* **2007**, *46*, 884. (b) Stamatatos, T. C.; Abboud, K. A.; Wernsdorfer, W.; Christou, G. *Polyhedron* **2007**, *26*, 2095.
(21) *S* = 73/2 Ge, C. H.; Ni, Z.-H.; Liu, C.-M.; Cui, A.-L.; Zhang, D.-Q.; Kou, H.-Z. *Inorg. Chem. Commun.* **2008**, *11*, 675.
(22) *S* = 37 Moushi, E. E.; Stamatatos, T. C.; Wernsdorfer, W.; Nastopoulos, V.; Christou, G.; Tasiopoulos, A. J. *Inorg. Chem.* **2009**, *48*, 5049.
(23) *S* = 83/2 (a) Ako, A. M.; Hewitt, I. J.; Mereacre, V.; Clérac, R.; Wernsdorfer, W.; Anson, C. E.; Powell, A. K. *Angew. Chem., Int. Ed.* **2006**, *45*, 4926. (b) Cremades, E.; Ruiz, E. *Inorg. Chem.* **2010**, *49*, 9641. (c) Mameri, S.; Ako, A. M.; Yesil, F.; Hibert, M.; Lan, Y.; Anson, C. E.; Powell, A. K. *Eur. J. Inorg. Chem.* **2014**, *2014*, 4326.
(24) (a) Rinehart, J. D.; Fang, M.; Evans, W. J.; Long, J. R. *Nat. Chem.* **2011**, *3*, 538. (b) Rinehart, J. D.; Fang, M.; Evans, W. J.; Long, J. R. *J. Am. Chem. Soc.* **2011**, *133*, 14236. (c) Jeon, I. R.; Park, J. G.; Xiao, D. J.; Harris, T. D. *J. Am. Chem. Soc.* **2013**, *135*, 16845. (d) Fortier, S.; Le Roy, J. J.; Chen, C. H.; Vieru, V.; Murugesu, M.; Chibotaru, L. F.; Mindiola, D. J.; Caulton, K. G. *J. Am. Chem. Soc.* **2013**, *135*, 14670. (e) Fatila, E. M.; Clerac, R.; Rouzieres, M.; Soldatov, D. V.; Jennings, M.; Preuss, K. E. *J. Am. Chem. Soc.* **2013**, *135*, 13298. (f) Demir, S.; Jeon, I.-R.; Long, J. R.; Harris, T. D. *Coord. Chem. Rev.* **2014**, *289*, 149. (g) Meihaus, K. R.; Corbey, J. F.; Fang, M.; Ziller, J. W.; Long, J. R.; Evans, W. J. *Inorg. Chem.* **2014**, *53*, 3099. (h) Demir, S.; Nippe, M.; Gonzalez, M. I.; Long, J. R. *Chem. Sci.* **2014**, *5*, 4701.
(25) Blondin, G.; Girerd, J. J. *Chem. Rev.* **1990**, *90*, 1359.
(26) (a) Drueke, S.; Chaudhuri, P.; Pohl, K.; Wieghardt, K.; Ding, X. Q.; Bill, E.; Sawaryn, A.; Trautwein, A. X.; Winkler, H.; Gurman, S. J. *J. Chem. Soc., Chem. Commun.* **1989**, 59. (b) Ding, X. Q.; Bominaar, E. L.; Bill, E.; Winkler, H.; Trautwein, A. X.; Drueke, S.; Chaudhuri, P.; Wieghardt, K. *J. Chem. Phys.* **1990**, *92*, 178. (c) Cotton, F. A.; Daniels, L. M.; Falvello, L. R.; Murillo, C. A. *Inorg. Chim. Acta* **1994**, *219*, 7. (d) Cotton, F. A.; Daniels, L. M.; Maloney, D. J.; Murillo, C. A. *Inorg. Chim. Acta* **1996**, *249*, 9. (e) Gamelin, D. R.; Bominaar, E. L.; Kirk, M. L.; Wieghardt, K.; Solomon, E. I. *J. Am. Chem. Soc.* **1996**, *118*, 8085. (f) Cotton, F. A.; Daniels, L. M.; Falvello, L. R.; Matonic, J. H.; Murillo, C. A. *Inorg. Chim. Acta* **1997**, *256*, 269. (g) Zall, C. M.; Zherebetskyy, D.; Dzubak, A. L.; Bill, E.; Gagliardi, L.; Lu, C. C. *Inorg. Chem.* **2012**, *51*, 728. (h) Zall, C. M.; Clouston, L. J.; Young, V. G.; Ding, K. Y.; Kim, H. J.; Zherebetskyy, D.; Chen, Y. S.; Bill, E.; Gagliardi, L.; Lu, C. C. *Inorg. Chem.* **2013**, *52*, 9216.
(27) (a) Bechlars, B.; D'Alessandro, D. M.; Jenkins, D. M.; Iavarone, A. T.; Glover, S. D.; Kubiak, C. P.; Long, J. R. *Nat. Chem.* **2010**, *2*, 362. (b) Neese, F.; Pantazis, D. A. *Faraday Discuss.* **2011**, *148*, 229.
(28) (a) Cotton, F. A.; Curtis, N. F.; Johnson, B. F. G.; Mague, J. T.; Wood, J. S.; Harris, C. B.; Robinson, W. R.; Lippard, S. J. *Science* **1964**, *145*, 1305. (b) Cotton, F. A.; Murillo, C. A.; Walton, R. A. *Multiple Bonds Between Metal Atoms*; Springer: New York, 2005. (c) Nguyen, T.; Sutton, A. D.; Brynda, M.; Fettinger, J. C.; Long, G. J.; Power, P. P. *Science* **2005**, *310*, 844.

DOI: 10.1021/jacs.5b08962
J. Am. Chem. Soc. 2015, 137, 13949−13956

(29) (a) Gambardella, P.; Rusponi, S.; Veronesse, M.; Dhesi, S. S.; Grazioli, C.; Dallmeyer, A.; Cabria, I.; Zeller, R.; Dederichs, P. H.; Kern, K.; Carbone, C.; Brune, H. *Science* **2003**, *300*, 1130. (b) Miyamachi, T.; Schuh, T.; Märkl, T.; Bresch, C.; Balashov, T.; Stöhr, A.; Karlewski, C.; André, S.; Marthaler, M.; Hoffmann, M.; Geilhufe, M.; Ostanin, S.; Hergert, W.; Mertig, I.; Schön, G.; Ernst, A.; Wulfhekel, W. *Nature* **2013**, *503*, 242. (c) Rau, I. G.; Baumann, S.; Rusponi, S.; Donati, F.; Stepanow, S.; Gragnaniello, L.; Dreiser, J.; Pamonteze, C.; Nolting, F.; Gangopadhyay, S.; Albertini, O. R.; Macfarlane, R. M.; Lutz, C. P.; Jones, B. A.; Gambardella, P.; Heinrich, A. J.; Brune, H. *Science* **2014**, *344*, 988.
(30) Cotton, F. A.; Daniels, L. M.; Matonic, J. H.; Murillo, C. A. *Inorg. Chim. Acta* **1997**, *256*, 277.
(31) Lee, D.; Krebs, C.; Huynh, B. H.; Hendrich, M. P.; Lippard, S. J. *J. Am. Chem. Soc.* **2000**, *122*, 5000.
(32) Powers, T. M.; Fout, A. R.; Zheng, S. L.; Betley, T. A. *J. Am. Chem. Soc.* **2011**, *133*, 3336.
(33) Eames, E. V.; Harris, T. D.; Betley, T. A. *Chem. Sci.* **2012**, *3*, 407.
(34) Zhao, Q. L.; Harris, T. D.; Betley, T. A. *J. Am. Chem. Soc.* **2011**, *133*, 8293.
(35) *APEX2*, v. 2009; Bruker Analytical X-Ray Systems, Inc.: Madison, WI, 2009.
(36) Scheldrick, G. M. *SADABS*, version 2.03; Bruker Analytical X-Ray Systems, Inc.: Madison, WI, 2000.
(37) Spek, A. L. *PLATON, A Multipurpose Crystallographic Tool*; Utrecht University: Utrecht, The Netherlands, 2010.
(38) Sheldrick, G. M. *SHELXTL*, version 6.12; Bruker Analytical, X-Ray Systems, Inc.: Madison, WI, 2000.
(39) Bain, G. A.; Berry, J. F. *J. Chem. Educ.* **2008**, *85*, 532.
(40) Chilton, N. F.; Anderson, R. P.; Turner, L. D.; Soncini, A.; Murray, K. S. *J. Comput. Chem.* **2013**, *34*, 1164.
(41) Cole, K. S.; Cole, R. H. *J. Chem. Phys.* **1941**, *9*, 341.
(42) (a) Aubin, S. M. J.; Sun, Z.; Pardi, L.; Krzystek, J.; Folting, K.; Brunel, L.-C.; Rheingold, A. L.; Christou, G.; Hendrickson, D. N. *Inorg. Chem.* **1999**, *38*, 5329. (b) Yang, P. *The Chemistry of Nanostructured Materials*; World Scientific: Singapore, 2003.
(43) Ward, M. D. *Chem. Soc. Rev.* **1995**, *24*, 121.
(44) (a) Zadrozny, J. M.; Xiao, D. J.; Long, J. R.; Atanasov, M.; Neese, F.; Grandjean, F.; Long, G. J. *Inorg. Chem.* **2013**, *52*, 13123. (b) Zadrozny, J. M.; Xiao, D. J.; Atanasov, M.; Long, G. J.; Grandjean, F.; Neese, F.; Long, J. R. *Nat. Chem.* **2013**, *5*, 577.
(45) Schulz, C. E.; Hu, C. J.; Scheidt, W. R. *Hyperfine Interact.* **2007**, *170*, 55.
(46) Hazra, S.; Sasmal, S.; Fleck, M.; Grandjean, F.; Sougrati, M. T.; Ghosh, M.; Harris, T. D.; Bonville, P.; Long, G. J.; Mohanta, S. *J. Chem. Phys.* **2011**, *134*, 174507.
(47) Dutta, S. K.; Ensling, J.; Werner, R.; Florke, U.; Haase, W.; Gutlich, P.; Nag, K. *Angew. Chem., Int. Ed. Engl.* **1997**, *36*, 152.
(48) The decrease in the $\chi_M T$ product as temperature increases from 50 to 300 K is likely the result of population of a very small fraction of the excited state $S = 17/2$.
(49) Chilton, N. F.; Anderson, R. P.; Turner, L. D.; Soncini, A.; Murray, K. S. *J. Comput. Chem.* **2013**, *34*, 1164.
(50) An alternative method of fitting the $\chi_M T$ data for **2** and **3** is by considering an $S = 17/2$ ground state. This will require an approximate value of g around $\sim 2.5-2.6$.
(51) (a) Stamatatos, T. C.; Poole, K. M.; Abboud, K. A.; Wernsdorfer, W.; O'Brien, T. A.; Christou, G. *Inorg. Chem.* **2008**, *47*, 5006. (b) Moushi, E. E.; Stamatatos, T. C.; Wernsdorfer, W.; Nastopoulos, V.; Christou, G.; Tasiopoulos, A. J. *Inorg. Chem.* **2009**, *48*, 5049.
(52) (a) Thomas, L.; Lionti, F.; Ballou, R.; Gatteschi, D.; Sessoli, R.; Barbara, B. *Nature* **1996**, *383*, 145. (b) Friedman, J. R.; Sarachik, M. P.; Tejada, J.; Ziolo, R. *Phys. Rev. Lett.* **1996**, *76*, 3830.
(53) Soler, M.; Wernsdorfer, W.; Folting, K.; Pink, M.; Christou, G. *J. Am. Chem. Soc.* **2004**, *126*, 2156.
(54) Hernández Sánchez, R.; Zheng, S.-L.; Betley, T. A. *J. Am. Chem. Soc.* **2015**, *137*, 11126.
(55) Vanquickenborne, L. G.; Haspeslagh, L. *Inorg. Chem.* **1982**, *21*, 2448.

DOI: 10.1021/jacs.5b08962
J. Am. Chem. Soc. 2015, 137, 13949−13956